Articles

Mechanism of Free Radical-Induced Hemolysis of Human Erythrocytes: Hemolysis by Water-Soluble Radical Initiator

Yukio Sato,* Shinya Kamo, Takeo Takahashi, and Yasuo Suzuki

Pharmaceutical Institute, Tohoku University, Aobayama, Aoba-Ku, Sendai 980-77, Japan

Received March 16, 1995[⊗]

ABSTRACT: Hemolysis of human erythrocytes induced by free radicals initiated from water-soluble, 2,2′-azobis(amidinopropane) dihydrochloride (AAPH) has been investigated. The formation of the radical detected as DMPO (5,5-dimethyl-1-pyrroline *N*-oxide) adduct depended on temperature and AAPH concentration in a similar manner as hemolysis. The curve for the formation of DMPO−radical adduct, however, did not correspond directly to the hemolysis curve. The product of thiobarbituric acid-reactive materials, which reflect the extent of lipid peroxidation, could not be related directly to the hemolysis curve, too. During the hemolysis, the fluidity of the erythrocyte membrane did not change in appearance. To study whether band 3 proteins participate in the hemolysis or not, eosin-5-maleimide (EMI)-labeled ghosts were incubated in the presence of AAPH. High molecular weight band 3 was formed, and the induced circular dichrosim spectrum of the bound EMI was changed, indicating a conformational change of band 3. It was observed that ascorbic acid suppressed the hemolysis and the oxidation of band 3 dose dependently to produce an induction period. This result shows that specifically blocking band 3 oxidation inhibits the hemolysis, despite lipid peroxidation. Further, it was observed that the EMI-labeled erythrocytes revealed distinct clusters by incubation with AAPH. This means a redistribution of band 3 proteins to form hemolytic holes in the membrane. However, the time course of the conformational change of band 3 during the redistribution was not also correspondent to the hemolysis curve. These results indicate that either lipid peroxidation or redistribution of oxidized band 3 is not attributed only by itself to the hemolysis. Thus, the hemolysis was interpreted by a simple competitive reaction model between lipid peroxidation and redistribution of oxidized band 3. This model explained well the hemolysis curves.

There are many questions concerned with the membrane structural changes that underlie the hemolytic event (Hoffman, 1992). The present study aims to consider the characteristics of free radical-induced hemolysis.

It is well-known that the hemolytic reaction results also from a nonenzymatic free radical-mediated oxidation of erythrocyte membranes (Fee et al., 1975; Sies, 1986). Thus, the oxidation of erythrocyte or its ghost membranes by free radicals has been used as a model for the oxidative damages of biomembranes (Chiu et al., 1982; Arduini et al., 1989). In the process of hemolysis, it is considered that free radicals generated in the aqueous and/or lipid phase attack the membrane to induce the chain oxidation of lipids and proteins. Yamamoto et al. (1985) reported that the amounts of spectrin and band 3 in ghosts decreased with the extent of oxidation and that the high molecular weight proteins formed parallel to reaction time. Becker et al. (1986) reported that the oxidation of spectrin by diamide reduces the ability of spectrin to bind protein 4.1 and thereby lowers its actin binding. In this reaction, the sulfhydryl groups derived from cysteine are oxidized to disulfide independent of generating radicals.

Band 3 in erythrocyte membranes plays an important role in a rapid exchange of HCO_3^- against Cl^- across the membrane (Passow, 1986; Salhany, 1990). Besides the mediation of the anion exchange, other possible functions of band 3 have been considered (Low et al., 1989; Mohandas et al., 1992). Band 3 serves as a major site of membrane−cytoskeletal interaction, a critical component in the regulation of glycolysis in the cell and a mediator of aged and/or damaged cell removal (Low et al., 1985; Schofield et al., 1992; Corbett & Golan, 1993). Such functions depend mainly on properties of the water-soluble cytoplasmic domain of band 3. In addition, the responsibility of band 3 for several types of hemolysis such as photolysis (Pooler & Girotti, 1986), immunolysis (Kannan et al., 1988), hyperthermic lysis (Lepock et al., 1989), glycerol lysis (Sauer, 1991), and osmotic lysis (Salhany et al., 1987; Sato et al., 1993) has been reported. However, properties of the change in band 3 during the hemolysis induced by radicals have not been known well. To study whether band 3 changes its structure during the radical-induced hemolysis, we have treated erythrocytes with an azo compound, 2,2′-azobis(amidinopropane) dihydrochloride, that generates free radicals by its unimolecular thermal decomposition.

In the process of the radical-induced hemolysis, we analyzed here the fluidity change of erythrocyte membranes

* To whom correspondence should be addressed. Phone: (81) 22-217-6832; Fax: (81) 22-217-6831.

[⊗] Abstract published in *Advance ACS Abstracts,* July 1, 1995.

0006-2960/95/0434-8940$09.00/0

by the ESR spectroscopic method by using spin probes and conformational change by CD spectrometry by labeling band 3 with eosin-5-maleimide. Comparing the hemolysis curves with the extents in the occurrence of radicals, the lipid peroxidation, and the conformational change of band 3, we propose here a reaction model of the free radical-induced hemolysis.

MATERIALS AND METHODS

Materials. AAPH[1] was obtained from Wako Pure Chemical Industries, Ltd. DETAPAC was from Tokyo Kasei Kogyo Co., Ltd. DMPO was purchased from Aldrich Chemical Co., Inc., and EMI was from molecular Probes, Inc. The fatty acid spin labels, 5- and 16-doxylstearic acids, were purchased from Aldrich Chemical Co. All other chemicals were of highest available commerical quality. Deionized glass-distilled water was used throughout. MES and HEPES were obtained from Dojindo Laboratory. Fresh human red blood cells treated with sodium citrate anticoagulant were gifts from the Miyagi Prefecture Red Cross Blood Center.

Spin Trapping. To 310 ideal milliosomolarity (mOsm) sodium phosphate buffer, pH 7.4, or 10% erythrocyte suspensions in the same buffer containing 50 mM DMPO and 1 mM DETAPAC was added AAPH ranging from 0 to 75 mM, and the mixture was incubated in the dark under various conditions. The formation of DMPO-radical adduct was monitored by ESR spectra.

Hemolysis Assay. Ten percent erythrocyte suspensions in the 310 mOsm phosphate buffer were incubated with various amounts of AAPH in the dark at appropriate temperatures. After centrifugation for 10 min at 750*g*, the degree of hemolysis (%) was determined from the absorbance of hemoglobin at 540 nm in the supernatant. The value of 100% hemolysis was determined from the supernatant of 1 volume of erythrocyte cells with 9 volumes of water incubated for 10 min at 37 °C.

Estimation of Lipid Peroxidation. The lipid peroxidation was estimated from TBA reaction by the method of Fee et al. (1975) as the following. Erythrocyte suspensions of 10% (1.5 mL) were diluted to 5 mL with the phosphate buffer, then 2.5 mL of this suspension was added to 1 mL of 12% trichloroacetic acid with vigorous mixing. After centrifugation, 2 mL of the supernatant was separated and reacted with 2.5 mL of 0.7% TBA for 15 min in a boiling water bath. TBA values were measured at 535 nm.

Preparation of Spin-Labeled Erythrocytes. Ten milliliters of spin-label in chloroform (2×10^{-4} M) was added to a flask and evaporated to form a thin film on the wall of the flask. Then, 5 mL of packed erythrocytes was added to the flask and incubated for 10 min at 37 °C. The spin-labeled erythrocytes were separated by centrifugation and were washed several times with 310 mOsm phosphate buffer to remove unbound spin-labels.

Preparation of EMI-Labeled Ghosts. Ghosts were prepared according to the procedure of Dodge et al. (1963) at 4 °C. Leaky ghosts were divided into two batches and incubated either with 5 mM HEPES/150 mM KCl, pH 7.4, or with 5 mM MES/150 mM KCl, pH 6.0, buffer for 1 h at 37 °C. Then, the ghosts (0.26 mg of protein/mL) were incubated with EMI solution (2×10^{-5} M) of pH 7.4 or 6.0 for 2 h at 37 °C in the dark, followed by washing several times with 5 mM HEPES/150 mM KCl buffer (pH 7.4) to remove unreacted EMI molecules. These washed ghosts were incubated in the pH 7.4 buffer at 37 °C for 1 h. Thus, two types of EMI-labeled ghost suspensions were obtained, referred to as pH 7.4-treated ghosts and pH 6.0-treated ghosts, respectively. When the ghosts were incubated with EMI solution at pH 7.4, EMI molecules bound to the membrane-spanning domain of band 3 (pH 7.4-treated ghosts). When the ghosts were incubated at pH 6.0, EMI molecules bound both the membrane-spanning and the cytoplasmic domains of band 3 (pH 6.0-treated ghosts) (Chiba et al., 1990).

Spectral Measurements. The absorption spectra were taken by a Hitachi 150-20 spectrophotometer. ESR spectra were measured in hematocrit capillary tubes by a JEOL JES-FE1X ESR spectrometer with a field intensity of 3290 G. The usual spectrometer settings were X-band; 100 kHz modulation amplitude, 6.3 G; microwave power, 4 mW; amplitude, $2-4 \times 1000$; response, 0.03−0.1 s; sweep time, 8−16 min. At these conditions, no power saturation effect was observed. The CD spectra were recorded by a Jasco J-720 spectropolarimeter. The observed CD spectra were expressed in terms of molar ellipticity, $[\theta]$, in deg·cm^2/dmol, calculated on the basis of the concentration of EMI. The protein concentration of erythrocyte ghosts was determined by the method of Lowry et al. (1951) using bovine serum albumin as the standard. The ghost suspension of 0.13 mg of protein/mL corresponded to 1×10^{-3} M. All of the spectra were recorded at room temperature.

Microscopic Observation of EMI-Labeled Erythrocytes. The red blood cells were washed two times with 0.9% NaCl followed three times with 310 mOsm phosphate buffer, and the cells were incubated with EMI solution of 2×10^{-5} M for 3 h in the dark at 37 °C. The cells were then washed twice with the same buffer to remove unreacted labels. The EMI-labeled erythrocytes were observed with a photomicroscope (Olympus BH-2) and with a confocal scanning laser microscope (Lasertec Co. Ltd., 1LM21H).

RESULTS

Spin Trapping of Radical Originating from AAPH. Figure 1(a) shows ESR spectra of DMPO−AAPH radical adducts in isotonic phosphate buffer (pH 7.4) containing a complexing ligand DETAPAC. The spectrum has 1:2:2:1 quartet pattern. The intensity of the signal resulting from the DMPO−radical adduct increased with increasing temperature and correlated well with the concentration of AAPH as shown in Figure 1(b). Variations of the AAPH concentration and temperature affected only the intensity of the ESR signal but not the spectral pattern. This fact shows that the radical generated from AAPH should be one species.

In Figure 2(a), the changes in the signal intensity at various temperatures are shown as a function of incubation time. The time course of the intensity could be expressed by a single exponential equation ($y = a(1 - e^{-kt})$), where a is a constant which depends on the initial concentration of AAPH. The rate constants, k, for the formation of the DMPO-radical

[1] Abbreviations: AAPH, 2,2′-azobis(amidinopropane) dihydrochloride; CD, circular dichroism; DETAPAC, diethylenetriaminepentaacetic acid; DMPO, 5,5-dimethyl-1-pyrroline *N*-oxide; EMI, eosin-5-maleimide; ESR, electron spin resonance; HEPES, *N*-(2-hydroxyethyl)-piperazine-*N*′-2-ethanesulfonic acid; MES, 4-morpholineethanesulfonic acid; SDS−PAGE, sodium dodecyl sulfate−polyacrylamide gel electrophoresis; TBA, thiobarbituric acid.

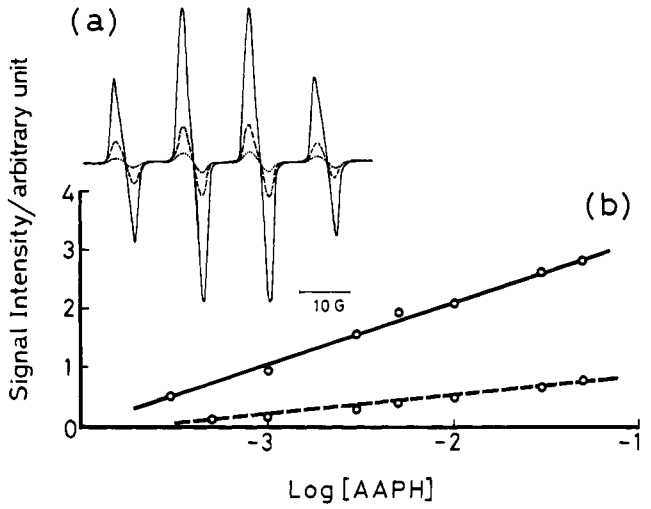

FIGURE 1: (a) ESR Spectra of DMPO–radical adduct at various temperatures. Reaction mixtures contained 1 mM DETAPAC, 30 mM AAPH, and 50 mM DMPO in the isotonic phosphate buffer, pH 7.4. (•••) 25 °C; (– –) 37 °C; (—) 45 °C. (b) Signal intensity of the DMPO-radical adduct plotted as a function of AAPH concentration in the isotonic phosphate buffer, pH 7.4. (- -O- -) 25 °C; (—O—) 37 °C.

adduct were calculated at various temperatures (Table 1). From an Arrhenius plot of these data, the activation energy of the formation of DMPO–radical adduct, E_a, was calculated to be 11.2 kcal/mol. The temperature dependence of the signal intensity (I) after 3 h incubation is shown in Figure 2(b) (solid line). A linear correlation was obtained. The radical generation was suppressed below about 10 °C.

In Figure 2(b), the temperature dependence of radical generation after 3 h incubation in the 10% erythrocyte suspensions is also presented (broken line). A slope of the line was parallel to that without erythrocytes, indicating that the species of radical in the AAPH–erythrocyte system was the same as that in the AAPH. Further, this line shifted to the higher temperature side. This suggests that a portion of free radicals originating from AAPH was consumed for physical state of erythrocyte hemolysis. Such consideration is consistent with the fact that spin trap reagents inhibit lipid peroxidation and hemolysis (Hill & Thornalley, 1983). In the presence of erythrocytes, the rate constants for the formation of the DMPO radical adduct slightly increased, as seen in Table 1. From an Arrhenius plot of these data, the activation energy of the formation of DMPO–radical adduct in the presence of erythrocytes was calculated to be 10.7 kcal/mol, which is nearly equal to that in the absence of erythrocytes.

Radical-Induced Hemolysis. Figure 3 shows hemolysis in the dark at 37 °C as a function of incubation time at various AAPH concentrations. The onset of hemolysis was delayed with the decrease of AAPH concentration, and the extent of hemolysis was proportional to the AAPH concentration (Figure 3 (inset)). A similar result was reported for rat erythrocytes by Miki et al. (1987). It should be noticed that the hemolysis curves in Figure 3 were sigmoid, though the generation curve of radical was hyperbolic (Figure 2). The hemolytic activity of AAPH increased with the increase of temperature. This corresponds to the temperature dependence of the radical generation shown in Figure 2(b).

Radical-Induced Oxidation of Membrane Lipids. Oxidative damage of membrane lipids and subsequent cross-linking

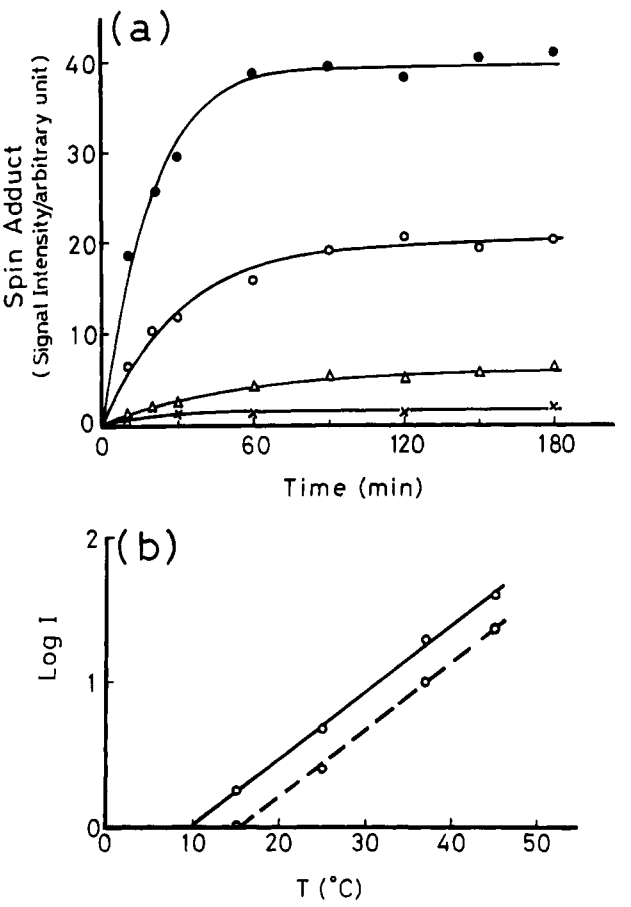

FIGURE 2: (a) Time course of the signal intensity derived from the DMPO-radical adduct in ESR spectra at various temperatures. Reaction mixtures contained 1 mM DETAPAC, 30 mM AAPH, and 50 mM DMPO in the isotonic phosphate buffer, pH 7.4. (×) 15 °C; (△) 25 °C; (○) 37 °C; (●) 45 °C. (b) Temperature dependence of signal intensity of DMPO–radical adduct. (—O—) Reaction conditions are the same as in (a), 180 min after incubation; (- -O- -) 10% erythrocyte suspensions in the same buffer, pH 7.4. Reaction conditions are the same as in (a), 180 min after incubation. Each point in (a) represents the average of 2 or 3 experiments.

Table 1: Rate Constants for the DMPO–Radical Adduct Formation (k) and for the Radical-Induced Change of Band 3 Conformation (k')[a]

T (°C)	k (min^{-1}) (in buffer)	k (min^{-1}) (in erythrocyte suspension)	k' (min^{-1})
15	0.008		0.011
25	0.020	0.019	0.016
37	0.034	0.048	0.031
45	0.055	0.061	0.053

[a] The data were obtained in isotonic phosphate buffer, pH 7.4. The values of k (in buffer) are estimated from the time courses in Figure 2(a).

of membrane proteins have been considered to be main reasons for hemolysis by free radicals (Chiu et al., 1982). It is well-known that TBA-reactive materials are formed in the lipid peroxidation process (Stocks & Dormandy, 1971), and the TBA value is used as an indicator.

Figure 4 shows time courses of TBA value (broken line), hemolysis (solid line), and formation of the DMPO–radical adduct in the presence of 10% erythrocytes at 37 °C (dotted line). The curves for the formation of radical and TBA-reactive materials do not directly correspond to the hemolysis curve. The time course of the radical generation was similar

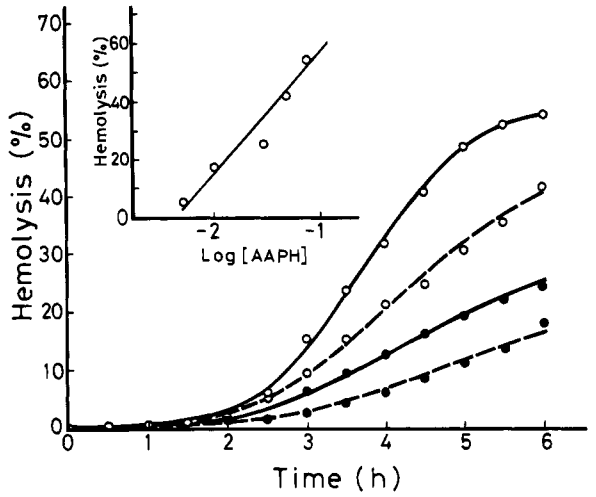

FIGURE 3: Time course of hemolysis of human erythrocytes in isotonic phosphate buffer (pH 7.4) in the presence of various amounts of AAPH at 37 °C. (- -●- -) 10 mM AAPH; (—●—) 30 mM AAPH; (- -○- -) 50 mM AAPH; (—○—) 75 mM AAPH. 10% erythrocyte suspensions were incubated in the presence of AAPH. Inset: Hemolysis after 6 h incubation at 37 °C was plotted against AAPH concentration. Each point represents the average of 3 experiments.

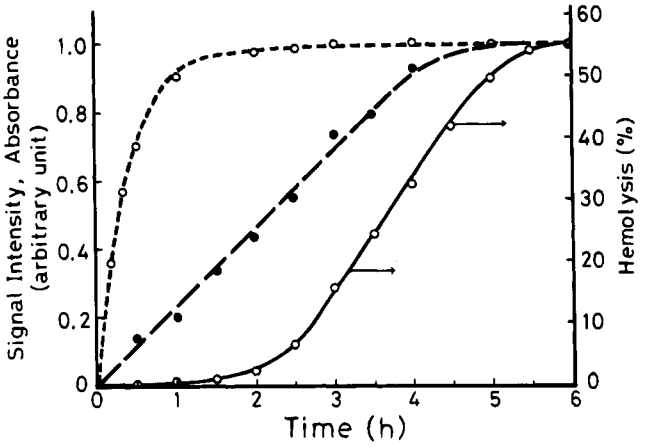

FIGURE 4: Relation of hemolysis to the formation of radical and the lipid peroxidation at 37 °C. (—○—) Time course of the hemolysis induced by radicals from AAPH (75 mM). (- - -○- - -) Time course of the signal intensity in ESR spectra by radicals in 10% erythrocytes; reaction mixtures contained 1 mM DETAPAC, 30 mM AAPH and 50 mM DMPO. (— —●— —) Time course of the TBA value by radicals from AAPH (75 mM) in 10% erythrocyte suspension. Each point represents the average of 2 or 3 experiments.

to that without erythrocytes as seen from Figure 2(a). A significant hemolysis occurred after the production of TBA-reactive materials reached a critical level (Stocks & Dormandy, 1971; Fee et al., 1975).

Next, a fluidity change of the erythrocyte membranes during the radical-induced hemolysis was examined by ESR spectra using 5- and 16-doxylstearic acids as probes. Figure 5 shows ESR spectra of 16-doxylstearic acids incorporated into erythrocyte membranes after various incubation times in the presence of AAPH. The spectra were progressively decreased and disappeared with incubation because of decomposition by free radicals from AAPH.

In Figure 6, changes in the spectral intensity of 5- and 16-doxylstearic acids are presented as a function of incubation time. The time courses for the intensity change of the central field peak (h_0) of 5- and 16-doxylstearic acids were

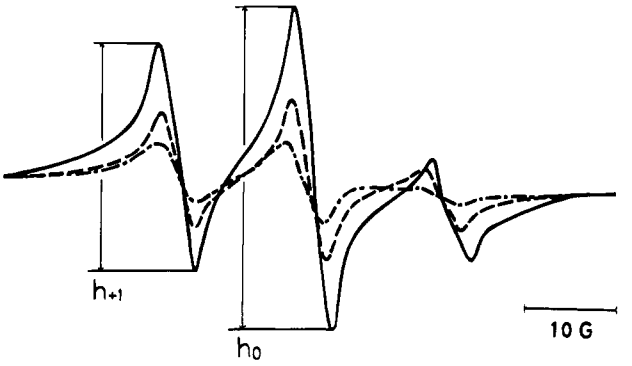

FIGURE 5: Change of ESR spectra of 16-doxylstearic acid incorporated into erythrocyte membranes in the presence of 30 mM AAPH at 37 °C. (—) immediately after an addition of AAPH; (— —) 30 min after incubation of 10% erythrocyte suspensions with AAPH; (— • —) 60 min after incubation of 10% erythrocyte suspensions with AAPH.

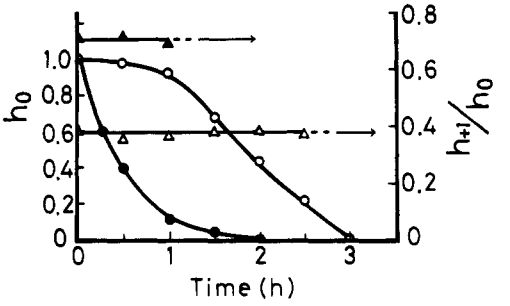

FIGURE 6: Intensity change in ESR signal derived from 5- and 16-doxylstearic acids incorporated into erythrocyte membranes at 37 °C after addition of 30 mM AAPH. (○) Time course of the intensity of the central field peak in ESR spectra of 5-doxylstearic acid. (●) Time course of the intensity of the central field peak in ESR spectra of 16-doxylstearic acid. (△) Change of the value of h_{+1}/h_0 in ESR spectra of 5-doxylstearic acid. (▲) Change of the value of h_{+1}/h_0 in ESR spectra of 16-doxylstearic acid. h_{+1}: intensity of the low field peak in ESR spectra; h_0: intensity of the central field peak in ESR spectra. Each point represents the average of 2 experiments.

different from each other. This indicates that the reactivity of the radicals with spin probes is dependent on the depth from the membrane surface. Near the head groups of the lipid bilayer, the time course of the intensity (spin probe—oxidation curve) was plotted as a sigmoidal curve, whereas in the hydrophobic end of the bilayer the spin probe—oxidation curve was hyperbolic. The probes near the hydrophobic end seem to be oxidized more rapidly than those near the head groups. A slight suppression of lipid peroxidation or protein oxidation by the spin probes may occur simultaneously, because an induction period in the hemolysis curve for the erythrocyte-embedded spin probes was slightly prolonged compared to that of intact erythrocytes (data not shown). This result is consistent with the report of Hill and Thornalley (1983).

Since the outer hyperfine splittings in ESR spectra of 5-doxylstearic acid were not well resolved, the fluidity change of the membranes was estimated by the use of h_{+1}/h_0 value, where h_{+1} indicates the height of the low field peak (Sato et al., 1978). The values of the h_{+1}/h_0 for 5- and 16-doxylstearic acids were scarcely influenced by the incubation of the erythrocytes with AAPH (Figure 6). In this connection, a second empirical parameter, the rotational correlation time (τ_c), was also calculated from spectra of 16-doxylstearic acid using peak intensity and line width (Schreier et al.,

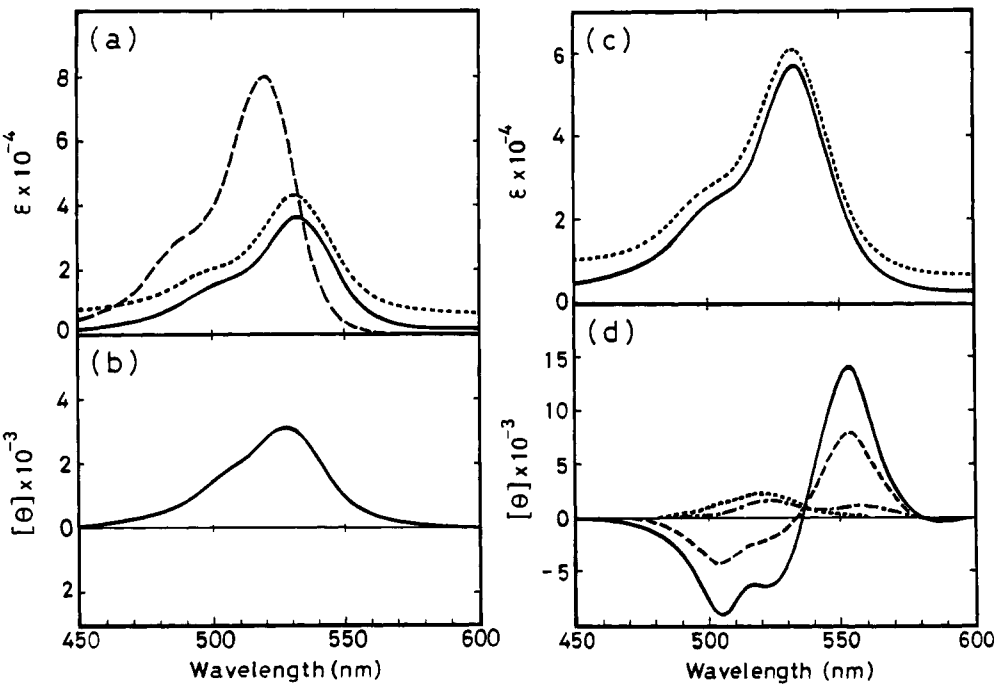

FIGURE 7: (a) Absorption spectra of EMI and EMI-labeled ghosts treated at pH 7.4. (– –) EMI alone at pH 7.4; (—) EMI-labeled ghosts immediately after an addition of 30 mM AAPH; (•••) EMI-labeled ghosts 180 min after incubation with 30 mM AAPH at 37 °C. (b) CD spectrum of EMI-labeled ghosts treated at pH 7.4. (c) Absorption spectra of EMI-labeled ghosts treated at pH 6.0. (—) EMI-labeled ghosts immediately after an addition of 30 mM AAPH; (•••) EMI-labeled ghosts 180 min after incubation with 30 mM AAPH at 37 °C. (d) CD spectra of EMI-labeled ghosts treated at pH 6.0 at various incubation times. (—) EMI-labeled ghosts in the absence of AAPH at 25 °C; (– –) after 20 min incubation in the presence of 30 mM AAPH at 37 °C; (– • –) after 120 min incubation in the presence of 30 mM AAPH at 37 °C; (•••) after 180 min incubation in the presence of 30 mM AAPH at 37 °C.

1978). The value of τ_c (~2.5 ns) was essentially unaffected 30 min after incubation. From these findings, it can be said that the physical properties of the erythrocyte membranes were not drastically disrupted by the radicals from AAPH, even though the peroxidation of the membrane lipids occurs. This indicates also that the lipid peroxidation is not predominantly responsible only by itself for the hemolysis by radicals.

Conformational Change of Band 3. When erythrocyte ghosts were incubated with AAPH, the bands of spectrin and band 3 in SDS–PAGE were decreased and high molecular weight proteins appeared with increasing incubation times, similar to the results reported by Yamamoto et al. (1985) (data not shown). When EMI-labeled ghosts were incubated with AAPH, EMI fluorescence could be detected both at the band of band 3 and at the top of the gel. Thus, band 3 may be cross-linked by incubation with AAPH, following which it becomes highly polymerized.

Then, we examined the change of band 3 structure. To study the structural change of band 3, two types of EMI-labeled ghosts, the pH 7.4- and pH 6.0-treated ghosts, were prepared as described in the Materials and Methods section. The absorption and CD spectra of the pH 7.4-treated ghosts are shown in Figure 7, panels (a) and (b), respectively. The absorption spectrum of EMI alone shows a band at about 519 nm and shoulder at about 485 nm at pH 7.4 (Figure 7(a) (broken line)). In the case of the pH 7.4-treated ghosts, the absorption maximum of EMI shifted to 532 nm with decreased intensity (Figure 7(a) (solid line)). Incubating the pH 7.4-treated ghosts with AAPH for 3 h, the spectrum changed its intensity (Figure 7(a) (dotted line)). This is due to an increase of light scattering resulting from the membrane oxidation by radicals. In Figure 7(b), a positive CD band similar to the absorption spectrum was observed at about 525 nm. This CD originates from EMI molecules bound to Lys-430 in the membrane-spanning domain of band 3 (Chiba et al., 1990; Cobb & Beth, 1990). The CD spectrum was not changed after incubation for more than 3 h in the presence of AAPH. These facts indicate that the microenvironment of the EMI binding site in the pH 7.4-treated ghosts was not influenced by the radicals generated from AAPH. This corresponds also to the fact that the physical properties of the membranes are not changed by the radicals.

The absorption spectra of the pH 6.0-treated ghosts were similar to those of the pH 7.4-treated ghosts except for their intensity (Figure 7(c) (solid line)). Also in this case, the spectrum was shifted upward after incubation with AAPH (Figure 7(c) (dotted line)). From Figure 7(a),(c), it can be said that the radicals from AAPH did not decompose EMI molecules bound to band 3.

The CD spectra of the pH 6.0-treated ghosts are shown in Figure 7(d). The CD spectrum was extremely different from that of the pH 7.4-treated ghosts. A positive CD band at about 552 nm and two negative bands at about 523 and 505 nm indicate that the microenvironment of the EMI binding site and the conformation of the bound EMI molecules are different from those in the pH 7.4-treated ghosts. In the case of the pH 6.0-treated ghosts, EMI molecules are considered to be located on the cysteine cluster in the cytoplasmic domain beside the Lys-430 (Chiba et al., 1990; Yamakose et al., 1993). As shown in Figure 7(d), the CD spectra of the pH 6.0-treated ghosts were drastically changed by incubation with AAPH. The final spectrum was in fair agreement with that of the pH 7.4-treated ghosts (Figure 7(d) (dotted line)). This suggests that some ordered structure of the cysteine cluster was destroyed by the radicals from

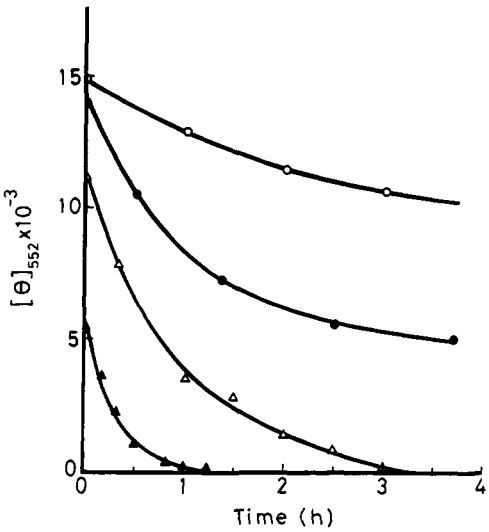

FIGURE 8: Time course of the intensity change in the CD spectra of EMI-labeled ghosts treated at pH 6.0 after incubation with 30 mM AAPH at various temperatures: (○) at 15 °C; (●) at 25 °C; (△) at 37 °C; (▲) at 45 °C. Each point represents the average of 2 or 3 experiments.

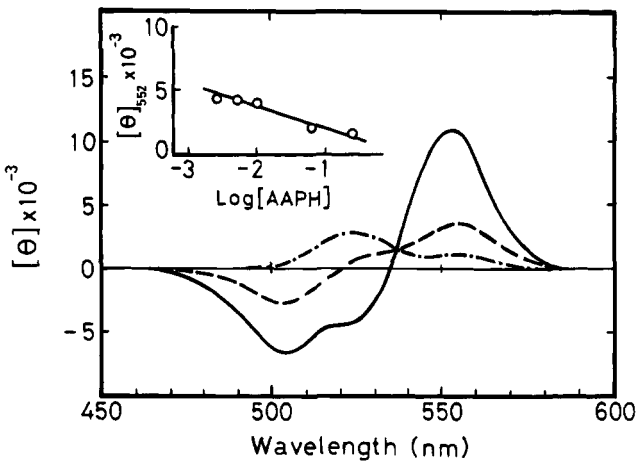

FIGURE 9: CD spectra of EMI-labeled ghosts treated at pH 6.0 after 3 h incubation with various amounts of AAPH at 37 °C. (—) in the absence of AAPH; (– –) 5×10^{-3} M AAPH; (– · –) 5×10^{-2} M AAPH. Inset: CD intensity of EMI-labeled ghosts treated at pH 6.0 after 3 h incubation at 37 °C plotted against AAPH concentration.

AAPH, whereas the microenvironment of the EMI binding site in the membrane-spanning domain remained unchanged as it is.

The changes in the CD intensity at the 552 nm band were plotted as a function of incubation time at various temperatures (Figure 8). The time course was hyperbolic. From these curves, the rate constants (k') for the change of band 3 conformation in the cytoplasmic domain were calculated (Table 1). The activation energy for the change was obtained to be 9.5 kcal/mol, which is comparable with that for the formation of DMPO–radical adduct.

Figure 9 presents an effect of AAPH on the CD spectral change of the pH 6.0-treated ghosts after 3 h incubation with various concentrations of AAPH. Similarly to Figure 7(d), an isoelliptic point was observed at about 537 nm, reflecting that two conformations of the cysteine cluster are responsible for the CD spectral change. In Figure 9 (inset), a linear correlation between the CD intensity at 552 nm and the concentration of AAPH is shown. By comparing this result

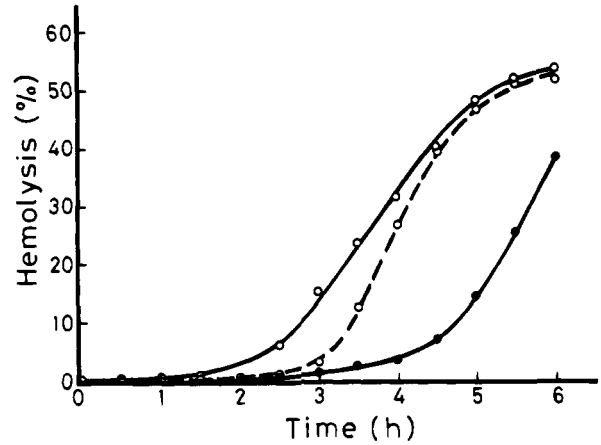

FIGURE 10: Time course of hemolysis of human erythrocytes in isotonic phosphate buffer (pH 7.4) at 37 °C in the presence of ascorbic acid. (—○—) In the absence of ascorbic acid; (– – ○– –) in the presence of 1×10^{-3} M ascorbic acid; (●) in the presence of 1×10^{-2} M ascorbic acid. [AAPH] = 75 mM. Each point represents the average of 3 experiments.

with that in Figure 3, we assumed that the conformation of the cysteine cluster was changed during the hemolysis. The formation of the polymerized form of band 3 should be accompanied by the conformational change of the cysteine cluster. Such changes of band 3 seem consistent with the fact that the cytoplasmic domain is apparently exclusively involved in the aggregation of the protein beyond the level of the stable dimer (Casey & Reithmeier, 1991).

Inhibition of Hemolysis by Ascorbic Acid. From the above-mentioned results, it is obvious that the membrane lipids and membrane proteins, especially band 3 and spectrin, are oxidized by the radicals from AAPH. Miki et al. (1987) and Niki et al. (1988) reported that α-tocopherol can suppress lipid oxidation but that it cannot prevent protein oxidation and hemolysis. We also obtained similar results to theirs. This indicates that either lipid peroxidation or protein oxidation is not attributed only by itself to the hemolysis. Thus, we examined effects of water-soluble antioxidants on hemolysis. The erythrocytes containing antioxidants were prepared as follows. Washed erythrocytes were incubated at 37 °C for 30 min in the presence of antioxidants of various concentrations. Then, the erythrocytes were washed to remove antioxidants that did not enter into erythrocytes. We studied effects of ascorbic acid, glucose, and glutathione on the hemolysis. Figure 10 shows hemolysis as a function of incubation time in the presence of ascorbic acid. The development of the hemolysis was prolonged as ascorbic acid concentration increased. Since ascorbic acid cannot stay within the membrane, its antioxidant activity cannot effectively prevent lipid peroxidation (Niki, 1991). The other two antioxidants did not suppress the AAPH-induced hemolysis. Ascorbic acid and glucose can easily cross the erythrocyte membrane or are transported by the carrier system (Rose, 1988; Janoshazi & Solomon, 1989). The rather stimulating effect of glucose may be due to free radicals and hydrogen peroxide produced by a glucose–glucose oxidation reaction. On the other hand, glutathione was not transported efficiently into cells (Meister, 1992), resulting in no suppression of hemolysis. Further, when erythrocyte ghosts containing ascorbic acid were incubated with AAPH, decrease of the spectrin and band 3 bands and increase of the high molecular protein band in SDS–PAGE

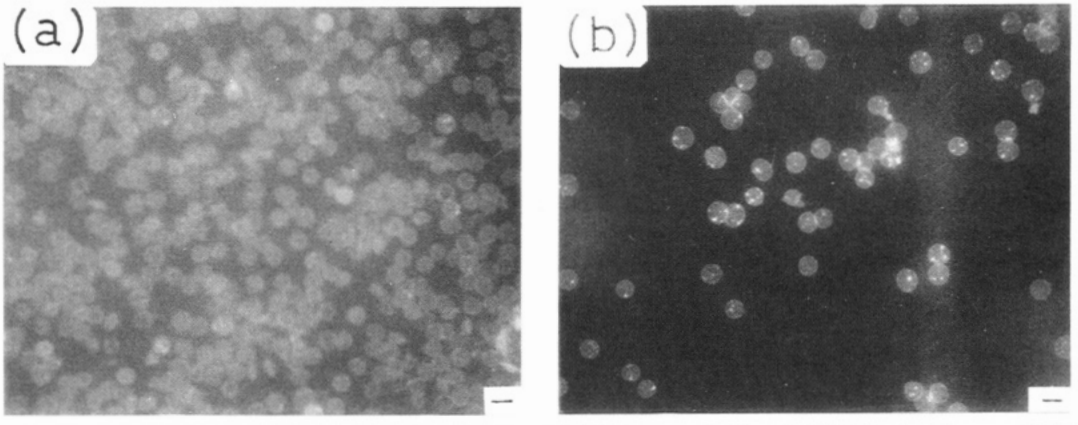

FIGURE 11: Fluorescence microscopy of erythrocytes labeled with EMI 4 h after incubation at 37 °C in the absence of AAPH (a) and in the presence of 75 mM AAPH (b). Scale bars = 10 mm.

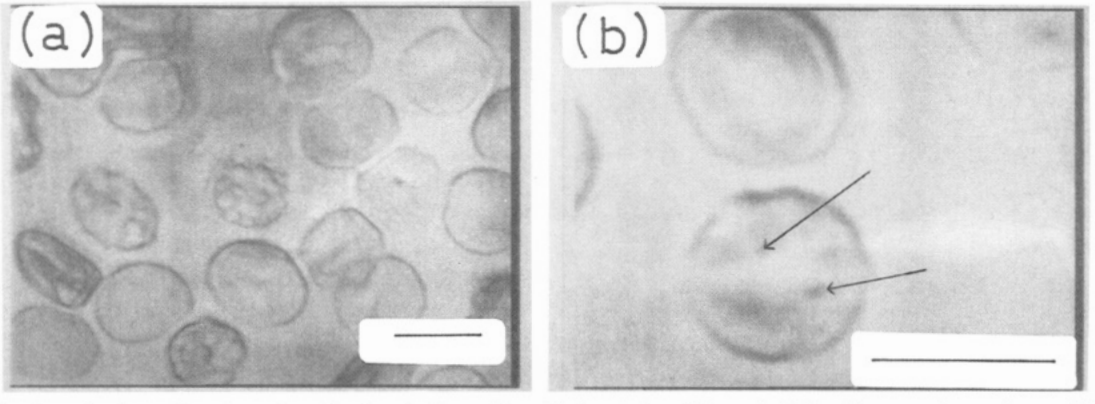

FIGURE 12: Surface structure of erythrocytes after incubation with radicals originated from AAPH: (a) gross observation and (b) hemolytic holes shown by arrows in an erythrocyte. The erythrocytes were incubated with 75 mM AAPH for 4 h at 37 °C and observed by a scanning laser microscope.

were suppressed (data not shown). These results indicate that a blocking of band 3 oxidation inhibits hemolysis.

Formation of Hemolytic Hole. To confirm a molecular association of band 3, a mobilization of band 3 during the hemolysis was examined by using EMI-labeled erythrocytes. Figure 11 shows the EMI-labeled erythrocytes 4 h after incubation at 37 °C. EMI fluorescence was observed over the entire surface of the erythrocytes in the absence of AAPH (Figure 11(a)), whereas distinct clusters of fluorescence appeared in an erythrocyte after incubation with 75 mM AAPH (Figure 11(b)). This indicates that band 3 proteins were topologically redistributed and clustered to form holes in the membrane.

Figure 12(a) represents surface structures of erythrocytes after incubation with AAPH. Biconcave discocyte was changed to sphere and/or echinocyte in the presence of AAPH. It can be said that a bulging of the erythrocytes is accompanied by redistribution of band 3 proteins. Further, a few holes per cell were formed (Figure 12(b)), corresponding to the band 3 clusters in Figure 11(b). The size and number of the hemolytic holes formed in an erythrocyte by AAPH are in contrast with those formed in a hypotonic hemolysis. In the hypotonic medium, each erythrocyte forms a single large hole in an erythrocyte membrane (Sato et al., 1993a,b).

DISCUSSION

Radicals Generated from AAPH. As seen from Figure 1(a), the ESR spectra of the DMPO−radical adduct in the aqueous solution showed a 1:2:2:1 quartet pattern, $A_N = A_H = 13.1$ G. This spectral pattern is similar to that of DMPO−OH ($A_N = A_H = 14.9$ G) (Finkelstein et al., 1980). DMPO can trap also nitrogen, halogens, and carbon. Further, a trapping of oxygen-centered radicals gives spectra similar to DMPO−OOH, consisting of a characteristic 1:1:1:1 quartet with hyperfine splitting (Finkelstein et al., 1980). ESR spectra of the DMPO-radical adduct could be obtained also in the absence of oxygen (data not shown). Thus, the DMPO-radical adduct observed in the present study should be DMPO−A$^\bullet$, where A$^\bullet$ corresponds to amidinopropane hydrochloride. Although AAPH is a water-soluble radical initiator, peroxy radicals formed in the nonpolar hydrocarbon interior of a bilayer diffuse into and preferentially reside in this region (Barclay & Ingold, 1981; Barclay et al., 1984). Furthermore, the hydrophobic region is expected to contain a large proportion of fatty acid double bonds susceptible to lipid peroxidation. Therefore, nitroxide radicals located in nonpolar regions are oxidized more rapidly by peroxy radicals than those located near polar head groups (Figure 6). Consequently, the mean course of the two spin probe−oxidation curves in Figure 6 can be compared with the curve for lipid peroxidation shown in Figure 4.

Influences of Radicals on Membrane Fluidity. In the present study, the apparent lack of change in membrane fluidity was observed. Concerning the membrane fluidity change by radicals, contradictory results were reported. Rice-Evans and Hochstein (1981) reported a decrease in bulk lipid fluidity following lipid peroxidation by phenylhydrazine. The

decrease of fluidity in peroxidative states was also reported by Dobretsov et al. (1977) and Barrow and Lentz (1981) in phospholipid vesicles and Eichenberger et al. (1982) in microsomal membranes. Bruch and Thayer (1983) found that the magnitude of the fluidity decrease in liposomes was markedly dependent on the intramembrane location. Watanabe et al. (1990) also studied a decrease in membrane fluidity of erythrocytes. In contrast with these reports, Grzelinska et al. (1979) reported that fluidity increased slightly following peroxidation of erythrocytes by γ radiation when 12-doxylstearic acid was used as the spin probe. They found, however, no change in fluidity when 5-doxylstearic acid was used. The present study showed that no change in the membrane fluidity was observed when 5- and 16-doxylstearic acids were used. Further, a disappearance of ESR signals of the spin probes observed here has not yet been reported in the other papers. Therefore, we can say that the changes in the membrane fluidity are dependent not only on the depth from the membrane surface but also on selecting of initiators to form varieties of reactive species. In those previous reports, the lipid peroxidations were initiated by hydrogen peroxide, hydroxyl radical, or superoxide anion. Thus, three contradictory results regarding the membrane fluidity change have been obtained. Such changes of the physical properties in membranes caused by various kinds of free radicals may play an important role in cell injury.

Kinetics of Hemolysis Induced by Radicals from AAPH. The hemolysis caused by radicals can be characterized mainly by two events: lipid peroxidation and redistribution of oxidized band 3 within the membrane. It should be noted that the time course of hemolysis is sigmoid, whereas the time courses of lipid peroxidation and conformational change of band 3 are not (Figures 3, 4, and 8). This indicates that the lipid peroxidation and the conformational change of band 3 are not separate events in the hemolysis. In other words, two elements are responsible for the hemolysis induced by radicals. The cells change their shape from biconcave discocyte to sphere during this stage, and the echinocytic cells were also found (Figure 12). The bulges may result from the redistribution of band 3 proteins and another high molecular weight protein, spectrin. Becker et al. (1986) reported that oxidative cross-linking of spectrin had a drastic effect on the ability to bind protein 4.1, whereas the oxidation had no effect on its ability to associate with ankyrin. It is considered that the association between band 3 and spectrin is mediated by ankyrin (Bennett & Stenbuck, 1980a,b). Therefore, the responsibility of spectrin for the hemolysis seems to be small. Details of the spectrin behavior, however, remain to be solved, because it is considered that spectrin damage may ultimately result in hemolysis (Becker et al., 1986).

By considering of the participation both of lipid peroxidation and band 3 oxidation in erythrocyte membranes, a competitive model for the hemolysis reaction by free radicals can be illustrated as follows:

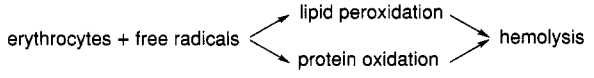

From the above-mentioned results, the binding of oxidized lipids to oxidized band 3 may occur. In the present study, however, the interaction between peroxidized lipids and oxidized band 3 is not taken into consideration for simplicity.

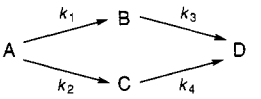

(1)

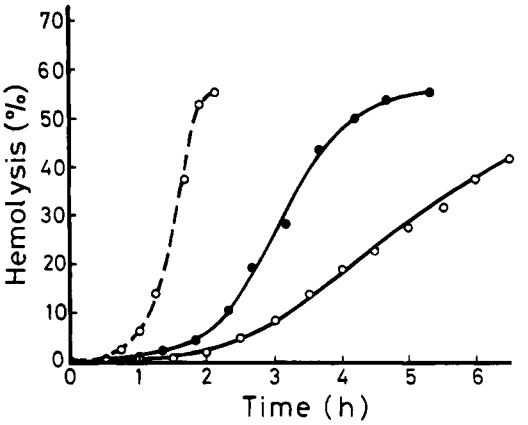

FIGURE 13: Curve fittings for the hemolysis by radicals originated from AAPH at various temperatures: (−○−) at 37 °C; (●) at 41 °C; (− −○− −) at 45 °C. The solid lines are the best fitted curves for the observed values by the use of eq 2 in the text. Each point represents the average of 2 experiments.

In this reaction, A, B, C, and D correspond to intact, swollen by lipid peroxidation, swollen by band 3 oxidation, and ruptured (hemolyzed) erythrocytes, respectively. k_1 and k_2 are rate constants for membrane swelling, and k_3 and k_4 are for membrane rupturing or forming of hemolytic holes. When [A], [B], [C], and [D] are substituted for the concentration of hemoglobin corresponding to each state, the integrated rate equation for [D] is as follows, from the boundary conditions, $[A] = [A]_0$ and $[B] = [C] = [D] = 0$ at $t = 0$:

$$[D] = [A]_0\left\{1 - \frac{k_1}{k_1 + k_2 - k_3}e^{-k_3 t} - \frac{k_2}{k_1 + k_2 - k_4}e^{-k_4 t} + \frac{k_1k_3 + k_2k_4 - k_3k_4}{(k_1 + k_2 - k_3)(k_1 + k_2 - k_4)}e^{-(k_1+k_2)t}\right\} \quad (2)$$

where $[A]_0$ is the initial concentration of hemoglobin. Thus, from eq 2, the relative values of the rate constant for the hemolysis induced by radical can be determined so as to give the smallest mean square error between observed and calculated values. The solid line in Figure 13 represents a computer fitting of hemolysis at various temperatures. The time course shown in Figure 13 seems to be explained well by eq 2. In this connection, the hemolysis curves in Figures 3 and 10 were the best fitted ones for the observed values drawn by using eq 2. The relative rate constants for the hemolysis at various temperatures obtained by eq 2 are presented in Table 2.

In the scheme in eq 1, it is necessary to decide which route corresponds to the lipid peroxidation or band 3 oxidation. The value of k_2 (or k_4) at 37 °C is most close to the value of k'. Thus, it can be considered that a route of A → C → D corresponds to the band 3 oxidation. The discrepancy between k_2 (or k_4) and k' should result from the difference in experimental conditions. That is, k' were obtained from the EMI−ghost system, whereas k_2 (or k_4) was from erythrocyte system. Furthermore, relative concentrations of AAPH to the lipid and membrane proteins in these systems

Table 2: Rate Constants for the Hemolysis Induced by Radicals Originated from AAPH[a]

T (°C)	k_1 (min^{-1})	k_2 (min^{-1})	k_3 (min^{-1})	k_4 (min^{-1})
32	0.080	0.033	0.117	0.017
37	0.165	0.052	0.223	0.021
	(0.164)	(0.019)	(0.182)	(0.014)
41	0.289	0.081	0.371	0.048
45	0.573	0.101	0.675	0.065

[a] The concentration of AAPH was 75 mM in 10% erythrocyte suspension. The values in parentheses are estimated from the hemolysis curve in Figure 10 in the presence of 10 mM ascorbic acid.

were different from each other. Since it can be postulated that binding affinities of peroxidized lipids to oxidized band 3 are different from those of intact lipids, boundary lipids around oxidized band 3 would be displaced by peroxidized lipids, which might promote a redistribution of band 3. The lipid peroxidation and band 3 oxidation are considered as the key elements of the hemolysis. Miki et al. (1987) reported that when high concentration of α-tocopherols were present, hemolysis still developed after an induction period depending upon the tocopherol concentration. This result seems to be similar to that of ascorbic acid addition (Figure 10). The relative importance of the two elements is not assessed in the present study. From Table 2, however, it is obvious that the rate-limiting step of hemolysis is a process of redistribution of oxidized band 3. The values of the rate constant in the presence of 10 mM ascorbic acid are listed in Table 2 (in parentheses). It is obvious that the process A → C → D was significantly suppressed, indicating an inhibition of hemolysis by blocking band 3 oxidation. This result also supports the competitive model.

An explanation of sigmoid curve and determination of the rate constant might be possible with other models. The most popular method to decide the rate of hemolysis is based on the slope of the percent hemolysis vs time curve, which is assumed to be sigmoid in character (Coldman & Good, 1968; Good, 1971). When hemolysis reaches 100%, the rate constant of hemolysis is given by $k = 50/t$, where t is the time when hemolysis reaches 50%. In this case, the values of the rate constant at various temperatures calculated using $k = 50/t$ were nearly equal to those of k_1 in Table 2. Consequently, it seemed that reliable values of the rate of hemolysis induced by radicals could not be obtained by this method. The equation based on the sequence X → Y → Z, where X, Y, and Z correspond to the intact erythrocytes, hemolyzing intermediates, and hemolyzed erythrocytes, respectively, could not fit the hemolysis data obtained in the present study (Anderson & Lovrien, 1977). The hemolysis curve is sigmoid in character. Such a curve can also be fitted with noncompetitive models. For example, an autocatalytic reaction model is able to fit the hemolysis data. However, this model is not adequate, because it requires merely one element.

The temperature dependence for hemolysis obeys the Arrhenius relation (Figure 14). The values of the activation energy for each process obtained from Figure 14 were listed in Table 3. The total of the activation energy is 93.3 kcal/mol. This value is larger than that in hyperthermia-induced hemolysis (72 kcal/mol) (Lepock et al., 1989). The difference may come from the fact that a coupling between peroxidized lipids and band 3 is necessary to the radical-induced hemolysis, whereas the hyperthermic hemolysis is due only to the denaturation of membrane proteins.

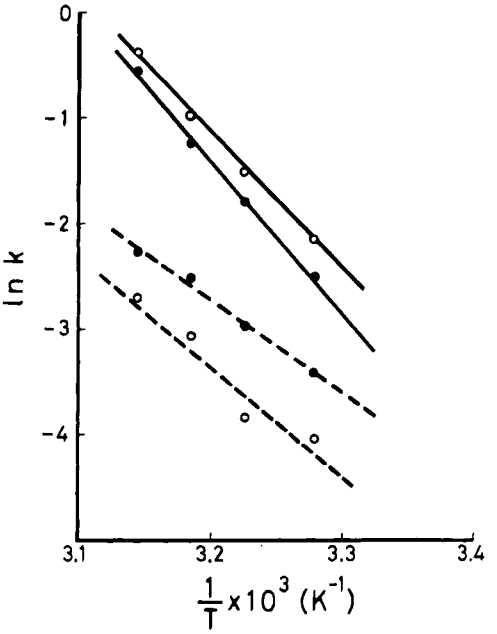

FIGURE 14: Arrhenius plots of the rate of hemolysis induced by radicals from AAPH at 37 °C. (—●—) k_1; (—○—) k_3; (– –●– –) k_2; (– –○– –) k_4.

Table 3: Activation Energy in Each Step for the Hemolysis Induced by Radicals Originated from AAPH

	lipid peroxidation		protein oxidation	
	A → B	B → D	A → C	C → D
E_a (kcal/mol)	28.9	17.1	25.8	21.5

The redistribution process should contain a spontaneous lateral diffusion within the membrane and an association and/or aggregation of oxidized band 3 (Liu et al., 1977). The value of E_a in the pathway C → D is larger than that in B → D. This might be due to the association of band 3 to form the hemolytic holes. In the aggregated state, the conformation of the cytoplasmic domain of oxidized band 3 is different from that of intact one. An accumulation of oxidized lipids around the aggregated band 3 may lead to the formation of hemolytic holes in the membrane. The interaction between peroxidized lipids and oxidized band 3 should be considered in detail. A study aimed at this point is in progress. In the present study, it is proposed that the radical-induced hemolysis can be explained well by the competitive reaction between lipid peroxidation and band 3 oxidation. Although the model proposed here seems oversimplified, the two elements are essential for the hemolysis induced by radicals.

REFERENCES

Anderson, P. C., & Lovrien, R. E. (1977) *Biophys. J. 20*, 181–191.

Arduini, A., Storto, S., Belfiglio, M., Scurti, R., Mancinelli, G., & Federici, G. (1989) *Biochim. Biophys. Acta 979*, 1–6.

Barclay, L. R. C., & Ingold, K. U. (1981) *J. Am. Chem. Soc. 103*, 6478–6485.

Barclay, L. R. C., Locke, S. J., MaccNeil, J. M., VanKessel, J., Burton, G. W., & Ingold, K. U. (1984) *J. Am. Chem. Soc. 106*, 2479–2481.

Becker, P. S., Cohen, C. M., & Lux, S. E. (1986) *J. Biol. Chem. 261*, 4620–4628.

Bennett, V., & Stenbuck, P. J. (1980a) *J. Biol. Chem. 255*, 2540–2548.

Bennett, V., & Stenbuck, P. J. (1980b) *J. Biol. Chem. 255*, 6424−6432.
Bruch, R. C., & Thayer, W. S. (1983) *Biochim. Biophys. Acta 733*, 216−222.
Casey, J. R., & Reithmeier, R. A. F. (1991) *J. Biol. Chem. 266*, 15726−15737.
Chiba, T., Sato, Y., & Suzuki, Y. (1990) *Biochim. Biophys. Acta 1025*, 199−207.
Chiu, D., Lubin, B., & Shohet, S. B. (1982) in *Free Radicals in Biology* (Pryor, W. A., Ed.) Vol. 5, pp 115−160, Academic Press, New York.
Cobb, C. E., & Beth, A. H. (1990) *Biochemistry 29*, 8283−8290.
Coldman, M. F., & Good, W. (1968) *Biochim. Biophys. Acta 150*, 194−205.
Corbett, J. D., & Golan, D. E. (1993) *J. Clin. Invest. 91*, 208−217.
Dobretsov, G. E., Borschevskaya, V. A., Petrov, V. A., & Vladimirov, Y. A. (1977) *FEBS Lett. 84*, 125−128.
Dodge, J. T., Mitchell, C., & Hanahan, D. J. (1963) *Arch. Biochem. Biophys. 100*, 119−130.
Eichenberger, K., Böhni, P., Winterhaltet, K. H., Kawato, S., & Richter, C. (1982) *FEBS Lett. 142*, 59−62.
Fee, J. A., Bergamini, R., & Briggs, R. G. (1975) *Arch. Biochem. Biophys. 169*, 160−167.
Finkelstein, E., Rosen, G. M., & Rauckman, E. J. (1980) *Arch. Biochem. Biophys. 200*, 1−16.
Good, W. (1971) *Exp. Physiol. Biochem. 4*, 163−181.
Grzelinska, E., Bartasz, G., Gwozdzinski, K., & Leyko, W. A. (1979) *Int. J. Radiat. Biol. 36*, 325−334.
Hill, H. A. O., & Thornalley, P. J. (1983) *Biochim. Biophys. Acta 762*, 44−51.
Hoffman, J. F. (1992) *Adv. Exp. Med. Biol. 326*, 1−15.
Janoshazi, A., & Solomon, A. K. (1989) *J. Membr. Biol. 112*, 25−37.
Kannan, R., Labotka, R., & Low, P. S. (1988) *J. Biol. Chem. 263*, 13766−13773.
Lepock, J. R., Frey, H. F., Bayne, H., & Markus, J. (1989) *Biochim. Biophys. Acta 980*, 191−201.
Liu, S.-C., Fairbanks, G., & Palek, J. (1977) *Biochemistry 16*, 4066−4074.
Low, P. S., Waugh, S. M., Zinke, K., & Drenckhahn, D. (1985) *Science 227*, 531−533.
Low, P. S., Willardson, B. M., Thevenin, B., Kannan, R., Mehler, E., Geahlen, R. L., & Harrison, M. (1989) in *Anion Transport Protein of the Red Blood Cell Membrane* (Hamasaki, N., & Jennings, M. L., Eds.) pp 103−118, Elsevier, Amsterdam.
Lowry, O. H., Rosebrough, N. J., Farr, A. L., & Randall, R. J. (1951) *J. Biol. Chem. 193*, 265−275.
Meister, A. (1992) *Biochem. Pharmacol. 44*, 1905−1915.
Miki, M., Tamai, H., Mino, M., Yamamoto, Y., & Niki, E. (1987) *Arch. Biochem. Biophys. 258*, 373−380.
Mohandas, N., Winardi, R., Knowless, D., Leung, A., Parra, M., George, E., Conboy, J., & Chasis, J. (1992) *J. Clin. Invest. 89*, 686−692.
Niki, E. (1991) *Am. J. Clin. Nutr. 54*, 1119S−1124S.
Niki, E., Komuro, E., Takahashi, M., Urano, S., Ito, E., & Terao, K. (1988) *J. Biol. Chem. 263*, 19809−19814.
Passow, H. (1986) in *Reviews of Physiology, Biochemistry and Pharmacology*, Vol. 103, pp 61−203, Springer-Verlag, Berlin and Heidelberg.
Pooler, J. P., & Girotti, A. W. (1986) *Photochem. Photobiol. 44*, 495−499.
Rice-Evans, C., & Hochstein, P. (1981) *Biochem. Biophys. Res. Commun. 100*, 1537−1542.
Rose, R. C. (1988) *Biochim. Biophys. Acta 947*, 335−366.
Salhany, J. M. (1990) in *Erythrocyte Band 3 Protein*, CRC Press, Boca Raton, FL.
Salhany, J. M., Raenbuehler, P. B., & Sloan, R. L. (1987) *J. Biol. Chem. 262*, 15974−15978.
Sato, B., Nishikida, K., Samuels, L. T., & Tyler, F. H. (1978) *J. Clin. Invest. 61*, 251−259.
Sato, Y., Yamakose, H., & Suzuki, Y. (1993a) *Biol. Pharm. Bull. 16*, 188−194.
Sato, Y., Yamakose, H., & Suzuki, Y. (1993b) *Biol. Pharm. Bull. 16*, 506−512.
Saur, A., Kurzion, T., Meyerstein, D., & Meyerstein, N. (1991) *Biochim. Biophys. Acta 1063*, 203−208.
Schofield, A. E., Tanner, M. J. A., Pinder, J. C., Clough, B., Bayley, P. M., Nash, G. B., Dluzewski, A. R., Reardon, D. M., Cox, T. M., Wilson, R. J. M., & Gratzer, W. B. (1992) *J. Mol. Biol. 223*, 949−958.
Schreier, S., Polnaszek, C. F., & Smith, I. C. P. (1978) *Biochim. Biophys. Acta 515*, 395−436.
Sies, H. (1986) *Angew. Chem., Int. Ed. Engl. 25*, 1058−1071.
Stocks, J., & Dormandy, T. L. (1971) *Br. J. Hematol. 20*, 95−111.
Watanabe, H., Kobayashi, A., Yamamoto, T., Suzuki, S., Hayashi, H., & Yamazaki, N. (1990) *Free Radical Biol. Med. 9*, 507−514.
Yamakose, H., Sato, Y., & Suzuki, Y. (1993) *Biol. Pharm. Bull. 16*, 1282−1287.
Yamamoto, Y., Niki, E., Eguchi, J., Kamiya, Y., & Shimasaki, H. (1985) *Biochim. Biophys. Acta 819*, 29−36.

BI950599T